Microwave Antenna for Microwave Magnetic Coupling to NV Centers in Diamond

EE491: B. Tech Project

Thariq Shanavas
150070058

Under the guidance of

Prof. Kasturi Saha
Prof. Pradeep Sarin

Department of Electrical Engineering
Indian Institute of Technology, Bombay
Mumbai 400076
November 17, 2018

Table of Contents

Abstract

The project broadly aims to improve upon NV center magnetometry by improving the uniformity of microwave excitation applied to the sample. Since the shot noise limited sensitivity improves as $1/\sqrt{N}$ where N is the number of NVs in the ensemble, providing a more uniform microwave excitation increases the size of the diamond sample, which in turn improves sensitivity.

This report presents microwave antennas as an alternative to loop-based microwave field generation techniques. Antenna models, design steps for tuning the antenna parameters, simulation tools and testing methods are described in this report. Finally, the report concludes with a critical analysis of earlier designs with the proposed antenna, and the expected improvement in shot-noise limited sensitivity.

List of Figures

Introduction

This Chapter briefly introduces Nitrogen Vacancy centers in Diamond, and touches upon the applications in Magnetometry. The later parts of the introductory chapter describes the optically detected magnetic resonance (ODMR) in NV, and the microwave coupling to the NV energy levels.

The Nitrogen Vacancy Centre in Diamond

The Nitrogen Vacancy is a point defect in diamond, with vast applications in quantum information and sensing. As far as this thesis is concerned, the property of interest in NVs is photoluminescence.

The nitrogen-vacancy center consists of a nearest-neighbor pair of nitrogen atom, which substitutes a carbon atom, and a lattice vacancy. A nitrogen atom has five valence electrons. Three of them covalently bond to the carbon atoms and two remain non-bonded and are called a lone pair. The vacancy has three unpaired electrons. Two of them make a quasi-covalent bond and one remains unpaired.

However, in the negative charge state N-V^-, an extra electron is located at the vacancy site forming a spin S=1 pair with one of the vacancy electrons. This charged N-V^- state is what is commonly, and somewhat incorrectly, called "the nitrogen-vacancy center".[1]

The electronic structure of the NV center is confirmed to be localized around the vacancy site and thus can be modelled by a molecular orbital in which the wavefunction is given by a linear combination of atomic orbitals (LCAO). The basis function of the molecular orbitals (MOs) is given by tetrahedrally coordinated sp^3 orbitals of dangling bonds of nearest three carbon atoms and the adjacent nitrogen atom.

The linear combinations of these carbon atoms and nitrogen atom form three MOs in the band gap (a_1, e_x, e_y) and one MO in the valence band (a_1'), given by

$$a_1 = \phi_N, a_1' = \frac{1}{\sqrt{3}S_1}(\phi_{C_1} + \phi_{C_2} + \phi_{C_3} - 3\beta\phi_N)$$

$$e_x = \frac{1}{\sqrt{3}S_2}(-\phi_{C_1} - \phi_{C_2} + 2\phi_{C_3}), e_y = \frac{1}{S_2}(\phi_{C_1} - \phi_{C_2})$$

$$S_1 = \sqrt{1 + 2\alpha - 3\beta^2}, S_2 = \sqrt{2 - 2\alpha}, \alpha = \langle\phi_{C_1}|\phi_{C_2}\rangle, \text{and } \beta = \langle\phi_{C_3}|\phi_N\rangle$$

The NV center consists of two electrons which fill the a_1 orbital and do not contribute to observable properties. Thus, the electronic configuration is represented by a configuration of four electrons filling the a_1, $e_{x,y}$ orbitals.

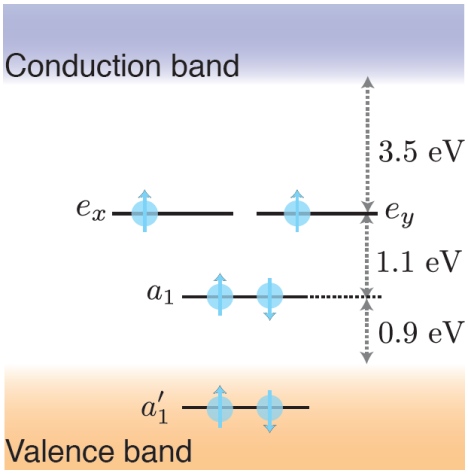

Figure 1: Molecular orbital models of the negatively charged NV center (six-electron model). The figure shows the configuration of the ground state 3A2 (a2 e2). All of the MOs are located far from conduction and valence bands and are well separated.

Ground State

The ground state of the NV is given by the electronic configuration $^3A_2$ ($a_1^2e^2$) with the spin triplet. The system may be effectively described by the spin operators of two unpaired electrons filling the $e_{x,y}$ orbitals. The dipole interaction between these two electrons induces an energy splitting (2.87 GHz) between the $m_s = 0$ and the $m_s = +/-1$ fine structure levels which quantizes the NV system along the [111] axis.[1]

The Hamiltonian of the ground state NV under a static magnetic field is given by

$$H = DS_z^2 + g\mu_B BS$$

Where D = 2.87 GHz is the zero field splitting constant, B is the static magnetic field along [1 1 1] and g_e = 2.0028 is the effective g-factor.

Excited State

The first excited state of the NV is given by $^3E(a_1e^3)$ with the spin triplet state and unlike the ground state, has an orbital doublet consisting of two unpaired electrons occupying a_1 and $e_{x,y}$. The fine structure of the excited state is experimentally confirmed to be very different for every NV center at low temperature and this is ascribed to the orbital structure being very sensitive to local strain which indeed splits the doubly degenerate orbitals. However, at room temperature, the phonon-related thermal excitations mix the orbital doublet without affecting spin projection component and thus the orbitals are averaged out into the singlet with zero orbital angular momentum. This quenching of the orbital angular momentum significantly simplifies the fine structure, enabling a model of the spin Hamiltonian with few parameters which has no variations among the NV centers.[1]

Intermediate State

There exist two singlet states with energy between the ground and the first excited states which both have the same orbital structure as the ground state. The transition between these two states are mainly driven by coupling to phonon vibrations associated with a weak infrared emission at 1042 nm (1.19 eV). The intermediate states are weakly connected to the triplet ground and excited states via the spin-orbit

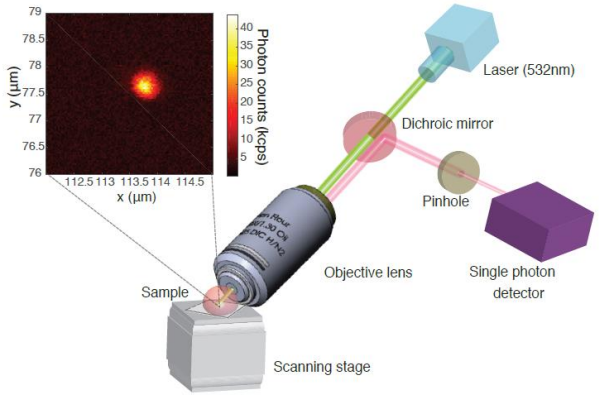

Figure 2: A scanning confocal microscope and its image of a single NV center. The diamond sample attached to the scanning stage is shined by the excitation laser at 532nm which is focused by the objective lens.

coupling and phonon coupling and this relaxation process preferably occurs at the excited states with m_s = +/-1, which then relaxes into the ground state with m_s = 0. Thus, the intermediate states play a crucial role in polarizing the state of the NV center.[1]

Fluorescence

Off-resonant illumination at 532 nm excites the ground state NV center to the first excited state. After losing energy to vibrational (phonon) excitations, the state is rearranged to $^3E(a^1e^3)$ and then decays into the ground state by spontaneous emission of photons at 637 nm.

At room temperature, the orbital part of the excited state is thermally mixed and the spin projection is preserved like the ground state. Thus, the rearrangement of the spin projection does not occur during the optical cycle. As a result, this off-resonant illumination between the spin triplets completely conserves the spin projection at room temperature. However, spin-orbit coupling in the excited state gives rise to intersystem crossing, i.e., transition between the triplet and the singlet states. The intersystem crossing preferably (six times more likely [2]) occurs in the m_s = +/-1 manifolds in the excited state. The intersystem crossing from the singlet to the ground triplet state occurs via coupling with phonons and experiment indicates that the spin preferably decays to m_s = 0 state. This spin-dependent and non-spin preserving relaxation process leads to polarization of the spin state into the m_s = 0 state (P ~ 80%) after a few optical cycles. The incomplete polarization is ascribed to the non-spin preserving transition between the two triplet states due to the spin-orbit coupling and a local strain. In addition, the transitions associated with the singlet states are not accompanied by emission of photons because they are driven by the spin-orbit coupling and the electron-phonon coupling. Since this non-radiative decay process depends on the initial spin state, the spin state can be correlated with the subsequent emission of photons after optical excitations.

Magnetometry

The ground state NV center spin can be manipulated by magnetic resonance techniques. Toward this purpose, in addition to a static magnetic field Bz along the [111] axis, an oscillating magnetic field B_1 with frequency ω is applied along the x direction.

Then, the Hamiltonian of the NV center is

$$H = DS_z^2 + g\mu_B B_z S_z + 2g\mu_B B_1 S_x \cos(wt)$$

where the oscillating field strength B_1 is much weaker than the transition frequency ($D \pm g\mu_B B_z S_z$). In order to obtain the time evolution of this time-dependent Hamiltonian, we describe the Hamiltonian in the frame rotating with frequency ω along the quantization axis (the so-called "rotating frame") by using the unitary transformation $U(t) = \exp(-i\omega S_z t)$:

$$\begin{aligned} \mathcal{H}_R &= U^\dagger(t)\mathcal{H}U(t) - i\frac{dU^\dagger(t)}{dt}U(t) \sim DS_z^2 + (g\mu_B B_z - \omega)S_z + g\mu_B B_1 S_x \\ &= \begin{pmatrix} D + g\mu_B B_z - \omega & \frac{1}{\sqrt{2}}g\mu_B B_1 & 0 \\ \frac{1}{\sqrt{2}}g\mu_B B_1 & 0 & \frac{1}{\sqrt{2}}g\mu_B B_1 \\ 0 & \frac{1}{\sqrt{2}}g\mu_B B_1 & D - g\mu_B B_z + \omega \end{pmatrix} \end{aligned}$$

With suitable approximations, H_R may be written as

$$\mathcal{H}_R = \frac{1}{2}(D + g\mu_B B_z - \omega)\sigma_z + \frac{1}{\sqrt{2}}g\mu_B B_1 \sigma_x$$

Where σ_z and σ_x are Pauli matrices. The initial state |0> evolves after a time τ under H_R becomes

$$\exp(-i\mathcal{H}_R\tau)U^\dagger(t)|0\rangle = \left\{\cos(\Omega'_e\tau) + i\frac{\Delta}{2\Omega'_e}\sin(\Omega'_e\tau)\right\}|0\rangle - i\frac{\Omega_e}{\sqrt{2}\Omega'_e}\sin(\Omega'_e\tau)|1\rangle$$

Where $\Omega'_e = \sqrt{\left(\frac{\Delta}{2}\right)^2 + \left(\frac{\Omega_e}{\sqrt{2}}\right)^2}$, $\Omega_e = g\mu_B B_1$ is the Rabi Frequency and $\Delta = D + g\mu_B B_z - \omega$ is the detuning from the resonant frequency. The transition probability $p(\tau)$ is given by

$$\begin{aligned} p(\tau) &= |\langle 1|U(t)\exp(-i\mathcal{H}_R\tau)U^\dagger(t)|0\rangle|^2 \\ &= \frac{1}{1 + (\frac{\Delta}{\sqrt{2}\Omega_e})^2}\sin^2\left(\sqrt{(\frac{\Delta}{2})^2 + (\frac{\Omega_e}{\sqrt{2}})^2}\tau\right) \end{aligned}$$

The transition probability is maximized on resonance Δ = 0 and suppressed when far off-resonant (Δ ≫ Ω). Thus, the smaller driving power (Ω_e) yields the narrower excitation profile and vice versa. This property is exploited for the selective excitation when the NV spin has several resonant frequencies due to the coupling to other electronic or nuclear spins.

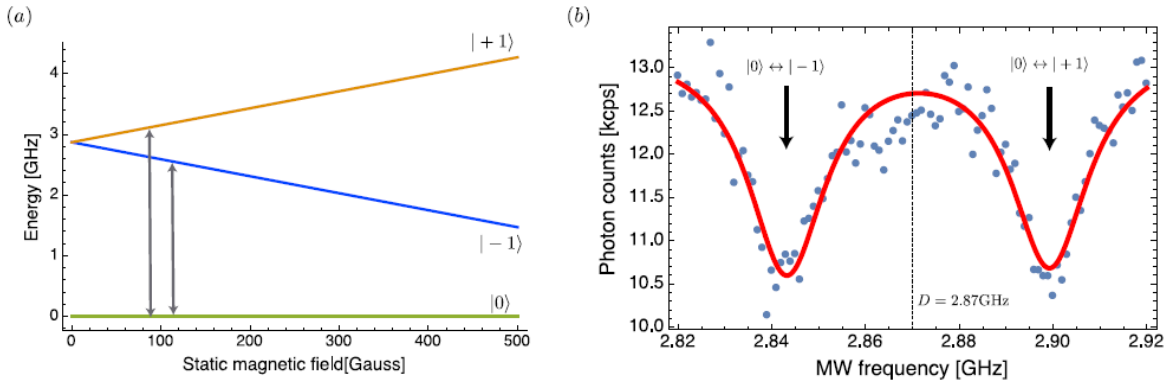

Figure 3: (a) Energy level of ground state NV. The degeneracy is lifted by static field along [111] axis by zeeman splitting. (b) CW-ODMR under ~10G. The two peaks correspond to transition between 0 and +/-1 levels.

Optically Detected Magnetic Resonance

In order to determine the resonance line, we employ continuous wave optically detected magnetic resonance (CW-ODMR). In the CW-ODMR measurement, the fluorescence is measured while a microwave (MW) field is continuously applied during the optical excitation at 532 nm. (Fig.2-6(b)). When the MW field is on resonance, the $m_s = 0$ state is mixed with the $m_s = +/-1$ states, resulting in a reduction of the fluorescence intensity. However, because of the overlap of the excitation and the detection processes, the linewidth is broadened (~ 10MHz) by the optical excitation and long excitation duration (few ms) and the sensitivity is limited. To sharpen the linewidth, the excitation process is isolated from the detection process. In addition, to enhance the selectivity of the resonance lines, a pulse-shaped MW field with a weak driving power is employed. This pulsed optically detected magnetic resonance (Pulsed-ODMR) technique attains much sharper line-width (few hundreds kHz) depending on the power of the MW field and the best contrast is obtained when the pulse length corresponds to a π rotation of the NV spin. The ODMR spectrum may be used to measure magnetic fields.

DC Magnetometry: ESR

The simplest method for measuring a magnetic field with NV centers is to take an ESR spectrum and extract the magnetic field information from the NV resonance frequencies. As described previously, in the presence of a magnetic field, the +/- 1 spin states – and subsequently the 0 to +/-1 transition frequencies of an NV center experience Zeeman splitting proportional to the magnetic field along the NV symmetry axis. A known static field can be applied along an arbitrary directions to distinguish four possible NV orientation classes from each other in a continuous wave electron spin resonance spectrum. Any additional δB results in net static field with ESR resonances shifted from those of the known B_0 spectrum. By extracting the resonance shifts which correspond to at least three of the four possible NV orientation classes, one can reconstruct the vector components of the unknown field.[3]

In addition, ESR may be performed using pulses. In pulsed ESR, a strong laser excitation first initializes the NV to the 0 state. Then a very low power MW pulse may rotate the NV into, for instance the |+1> state if the MW frequency is resonant with the |0> to |+1> spin transition. Finally a second short laser

excitation pulse is applied and the resulting fluorescence intensity is read out to determine the NV spin state. [3]

By sweeping the MW frequency, a spectrum similar to what is measured for CW-ESR scheme is extracted; however since for pulsed ESR, the optical excitation and MW radiation are not applied simultaneously and are therefore not competing, the MW power may be lower than in the CW-ESR scheme, thus reducing MW power broadening. Also, the optical power may be stronger than in the CW-ESR scheme, thus increasing the number of photons collected per measurement.

Ramsey: [3], Page 53.

Microwave coupling to the NV Centre

Since the Ramsey sequence requires that the same $\frac{\pi}{2}$ pulse be delivered to all NVs in the ensemble, it is critical that the microwave delivery is uniform for as large a sample size as possible.

The microwave field is typically delivered by loop-like structures in a PCB, and the diamond sample is placed on the PCB. Recent literature has used microwave antennas instead of current loops to deliver the magnetic field much more efficiently.

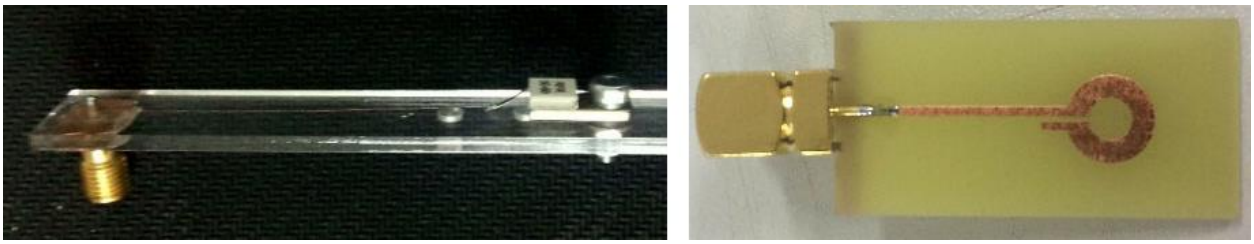

Figure 4 Copper wire and microstrip antenna from [6]

Literature Review

In recent years, several attempts have been made to utilize microwave antennas to deliver the magnetic field to the NV over current loops or wires [4], [5], [6].

In [6], the ODMR spectra using a microstrip antenna is reported to have 5 times better contrast than a wire antenna under similar conditions. The paper compares a copper wire antenna and a microstrip antenna in terms of frequency and impedance matching, near field radiation distribution, spin excitation performance, smith chart and electron spin resonance. The paper recommends the microstrip antenna over the copper wire antenna.

The microstrip antenna was reported to show decresed deviation from the impedance matching and better transmission efficiency as compared to the wire antenna, while at the same time showing improved ODMR concentration.

An SMA connector was used as the feed end to connect the microwave source. The end of the copper wire antenna is connected with a 50Ω radiofrequency resistance for impedance matching. The entire structure is fixed on an organic glass base to minimize the influence of microwave radiation from the materials. For the microstrip antenna, the entire structure was sputtered onto a printed circuit board made of a glass-epoxy (FR4) dielectric material.

The copper wire has few design constraints – analytical expressions for the resonant frequency are readily available. The microstrip antenna on the other hand is better designed using numerical toolkits. [6] used Ansys HFSS for simulations of the near field and resonant frequency. The paper also briefly touches upon vector magnetometry using an additional static field.

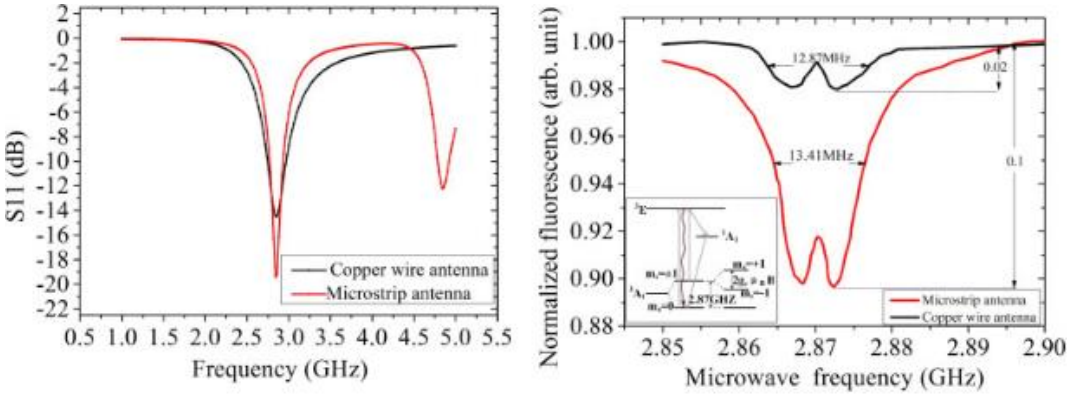

Figure 5: S11 parameter (left) and ODMR Spectrum

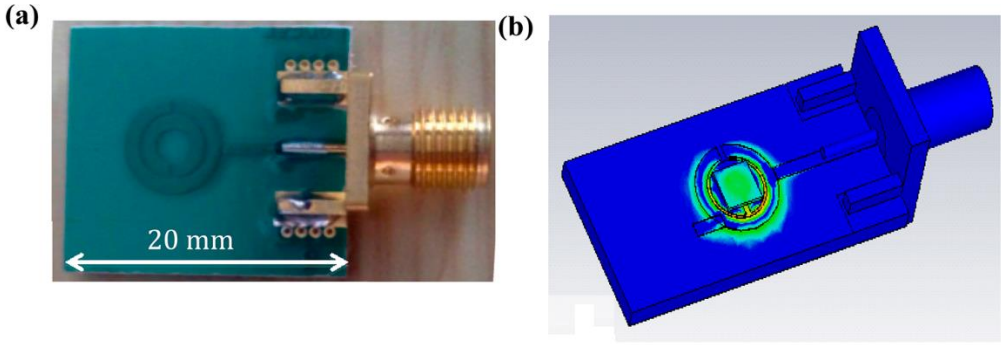

Figure 6: Double split ring resonator from [4]. Numerical simulation from CST Microwave Studio (Right)

[4] reports a double split ring resonator to deliver a uniform field over a mm^2 range area.

Uniformity and magnitude of delivered microwave field were measured using the Rabi nutation experiment on arrays of diamond nanowires with ensemble NV centers. An average Rabi nutation frequency of 15.65 MHz was measured over an area of 0.95 × 1.2 mm, for an input microwave power of 0.5 W. By mapping the Rabi nutation frequency to the magnetic field, the average value of the magnetic field over the aforementioned area and input microwave power was 5.59 G with a standard division of 0.24 G.

The analytical expressions governing the resonant frequency of the double split ring resonator is described in [7]. The analytical expressions were used as a starting point and the parameters were fine-tuned using CST Microwave studio. The variation of Hz along x, y, and z directions over 1.5 × 1.5 mm area and thickness of 0.5 mm is reported to be less than 6.5%, 10%, and 1%, respectively.

The diamond samples were divided into separate regions and the Rabi frequency was measured by spanning the confocal microscope. The microwave power was determined to be 5.59 G with a standard division of 0.24 G, using the relation $\Omega_{rabi} = \gamma B_1$ where $\gamma = 2.8\ MHz/G$. The reported usable area is around 1.14 mm^2. The Substrate used was a proprietary material from Rogers.

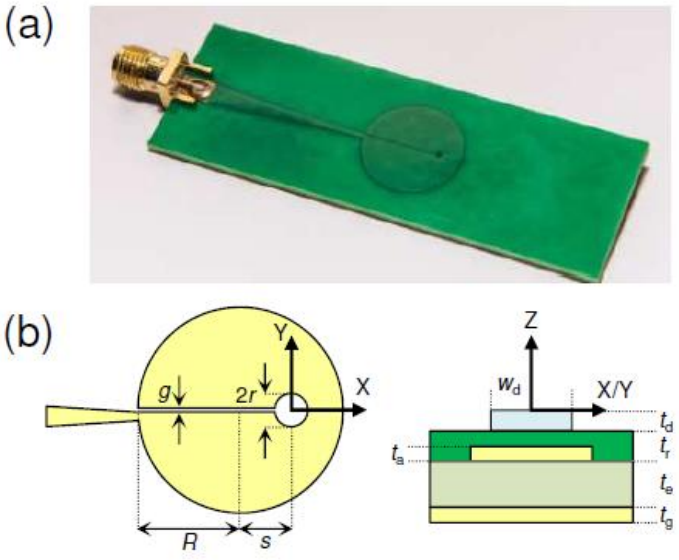

Figure 7: Microwave antenna from [5]

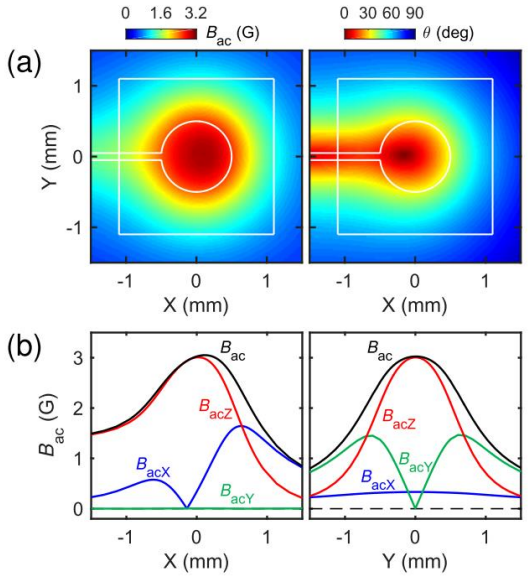

Figure 8(a) Contour plot of Bz along the xy plane, 0.5 mm above the surface of the PCB. Theta is angle from normal. (b) Variation along x and y axes, 0.5 mm above the PCB

[5] reports on a microwave planar ring antenna specifically designed for optically-detected magnetic resonance (ODMR) of nitrogen-vacancy (NV) centers in diamond. It has the resonance frequency at around 2.87 GHz with the bandwidth of 400 MHz, ensuring that ODMR can be observed under external magnetic fields up to 100 G without the need of adjustment of the resonance frequency. It is also spatially uniform within the 1-mm-diameter center hole (0.78 mm^2). FR-4 substrate was used for the PCB. The practicability of the design is verified using CW-ODMR, Pulsed ODMR and Rabi oscillations.

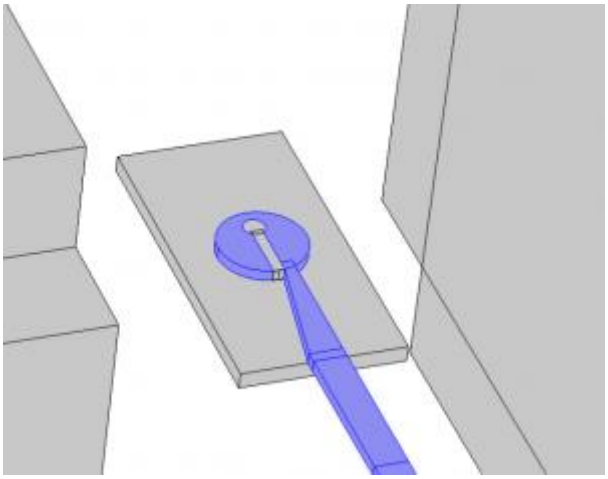

Figure 9 COMSOL model of microstrip antenna

Microstrip antenna

Sasaki et al[5] describes a microwave planar ring antenna specifically designed for optically detected magnetic resonance (ODMR) of nitrogen-vacancy (NV) centers in diamond. Since the design had few parameters and was easily fabricated on FR-4, the first round of PCBs were made after Sasaki's model.

Simulations

Since the substrate thickness at the PCB lab was different from the one used in the paper, some tuning would be required to replicate the result. I attempted to reproduce the results of the simulation before printing the PCB using COMSOL.

Within the AC/DC module, the magnetic and electric fields study was used, since it was most suited to voltage-excited systems with specific geometries (instead of generic multi-loop coils). The 'Terminal' boundary was used to excite the system with a 0.1 V sinusoidal signal at 2.8 GHz.

The system can be thought of as an LC oscillator. The inductance is provided by the circular hole and the capacitance by the rectangular gap in the middle. The magnetic field in the z-direction is expected to peak in the circular hole, and the electric field would be mostly constrained to the rectangular slit.

Results

The magnetic field along the z-direction was measured along the x, y and z-axes.

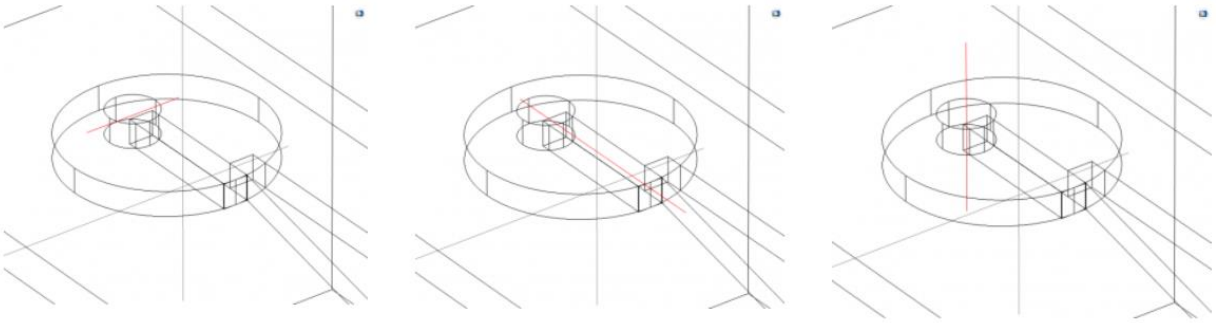

Figure 10: x, y and z axis of the simulation

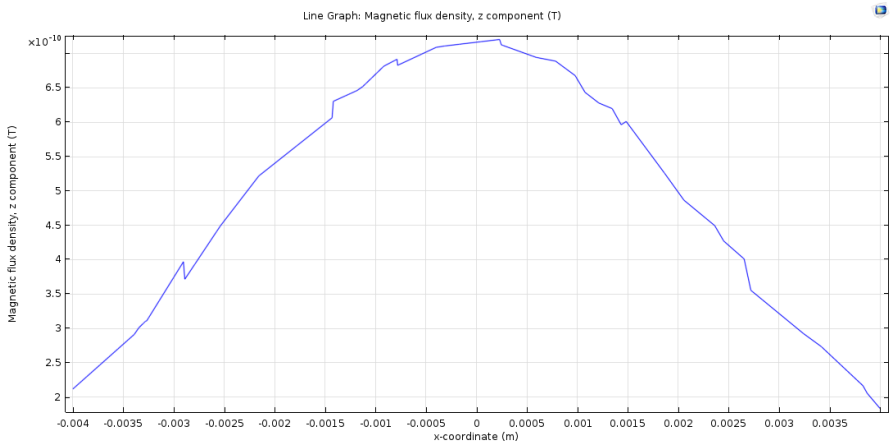

Figure 11 Bz along the x-axis, with z coordinate 0.5mm above the plane.

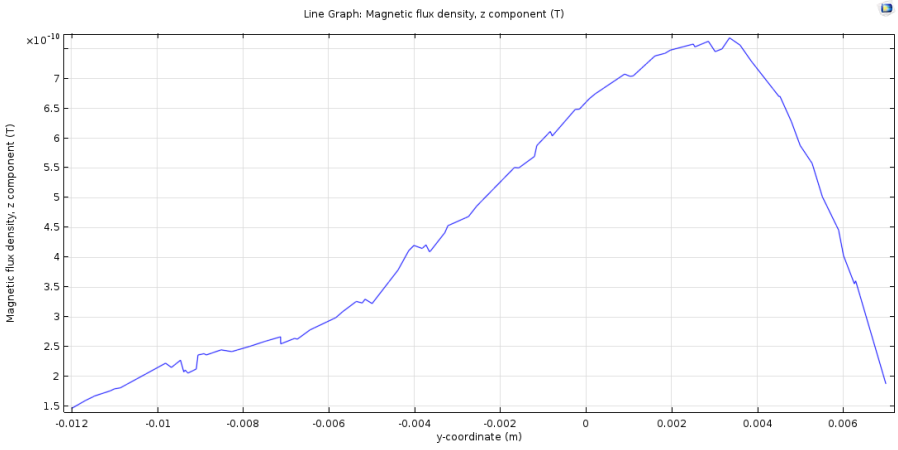

Figure 12 Bz along the y-axis, with z coordinate 0.5mm above the plane.

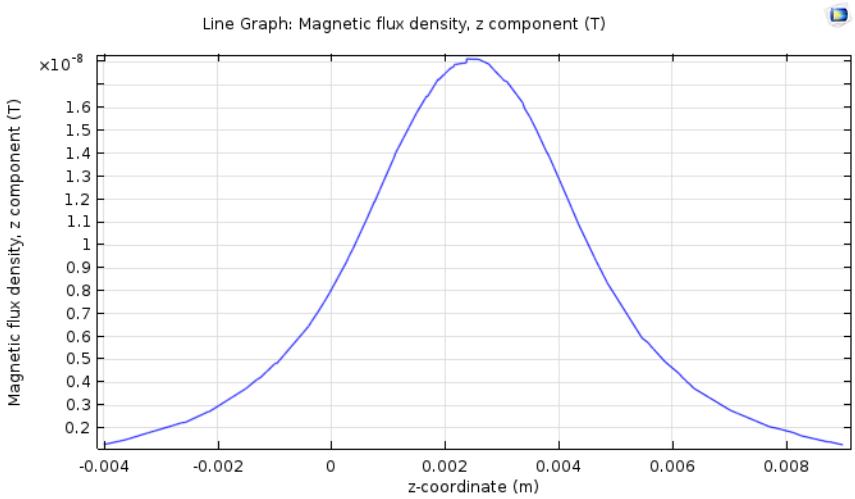

Figure 13 Bz along z axis

Figure 14 Fabricated PCB

Testing

The PCB was fabricated in the Rapid Prototyping PCB facility in the EE Department (annex Building, first floor) through chemical etching.

The ~26 mm feed line acts as a Quarter Wave transformer. The Quarter wave transformer matches the impedance of the loop to the instrumental 50 Ohm. The impedance matching was tested using a network analyser at the Antenna Lab.

The Network analyser sweeps frequency range from 2.5GHz to 3GHz – The antenna was expected to resonate at ~2.87GHz. It then plots the S parameter as a function of frequency.

The S11 parameter is closely linked to how much power is radiated by the antenna. For instance, if the S11 value is -10 dB and a power of -3dB is fed into the antenna, -13dB of power will be reflected back to the source. The rule of thumb says that for a good antenna design, the S11 parameter should be below -10 dB.

The current design was found to show a resonance (-5.4dB) at 2.99GHz.

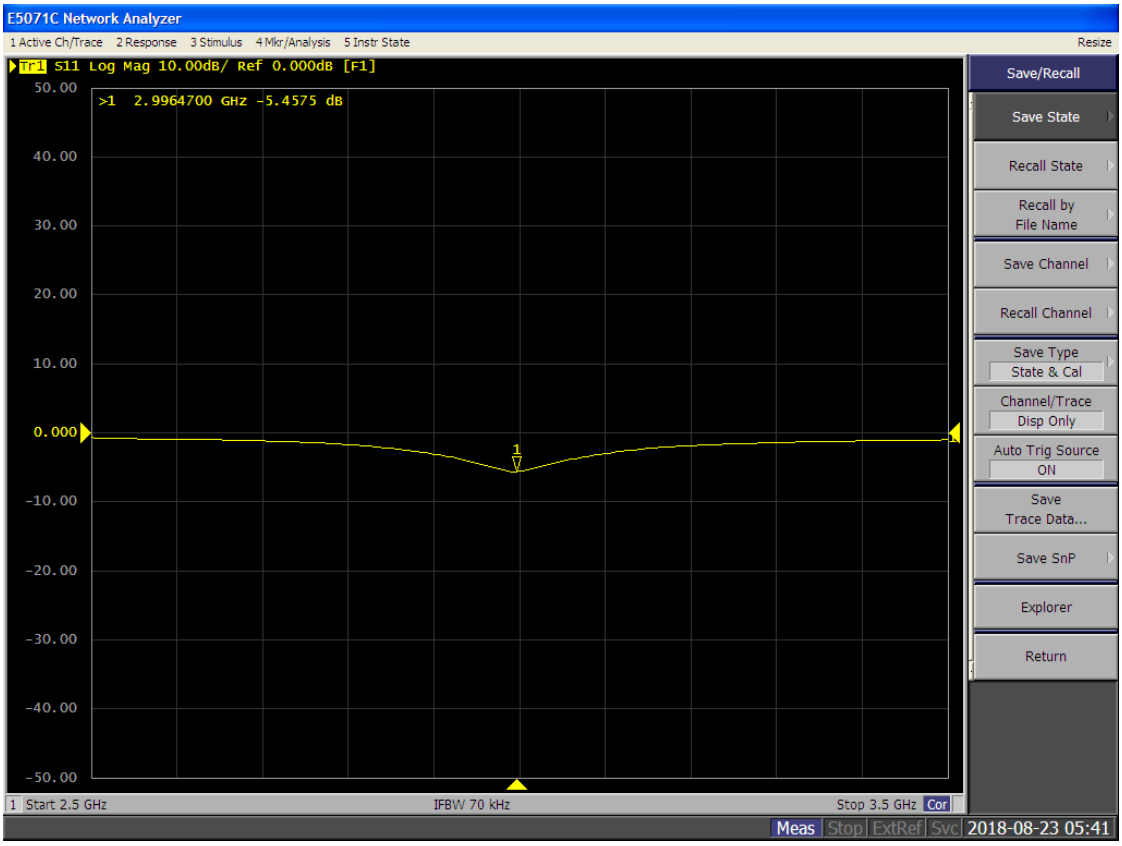

Figure 15 Observed S11 parameters as a function of frequency, from 2.5 to 3 GHz

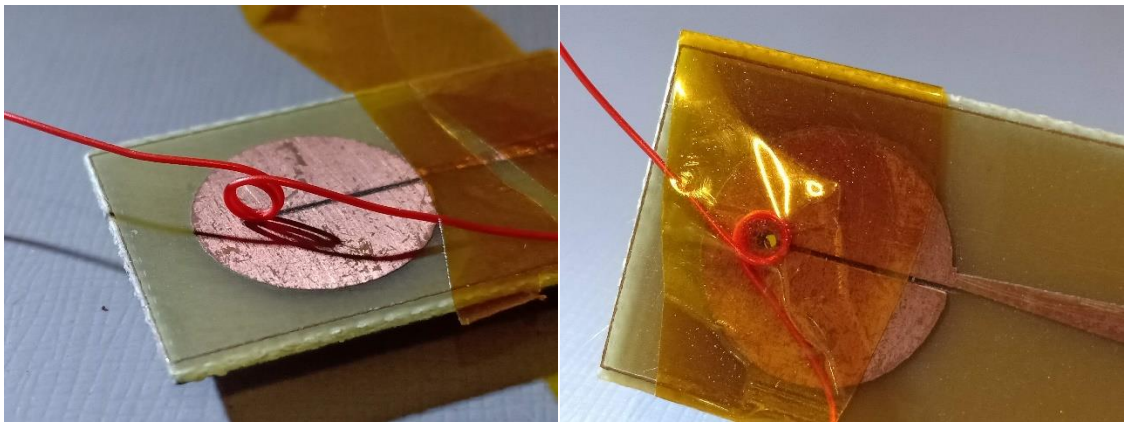

Setup for probing magnetic field along xy-plane (left) and z axis.
A non-conductive tape has been used to secure the loop in place on right.

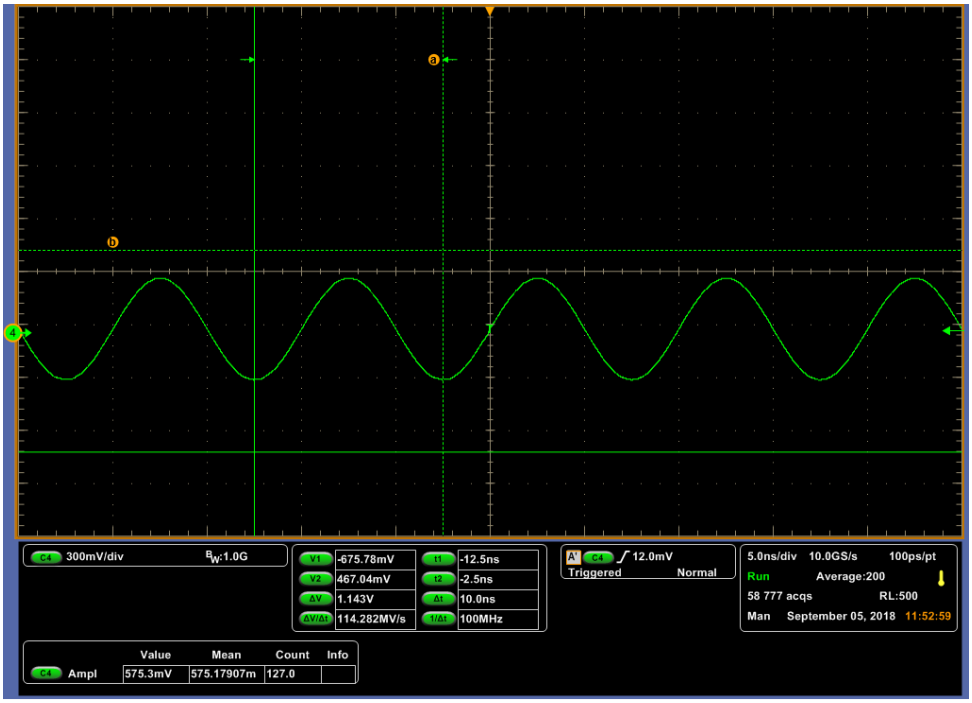

Figure 16 For 4 Vpp at 100 MHz, the electric field picked up by the oscilloscope (for coil in xy plane) Notice that the frequency of oscillation is 100MHz. The amplitude is 575 mV. This corresponds to a magnetic field of 0.7 G. Please note that the antenna itself isn't tuned for 100 MHz – The field strength is expected to be much stronger at 2.87 GHz. The experiment was repeated for 50MHz

Characterization of field

To get a first estimate of the field strength, a small loop was used to induce voltage.

Due to the instrumental limitation, the device was tested only up to 100MHz. This is indeed expected to have impedance mismatch issues (since the antenna was tuned to 2.9GHz). However, the B-field distribution should not be affected by impedance mismatch. The field was probed by the voltage induced in a two-loop coil of diameter 2.05mm.

By Faraday's law, the EMF induced would be, (for n turns of the coil and loop radius r)

$$E = -n\frac{d\phi}{dt}$$

$$E = -n * \pi r^2 \frac{dB}{dt}$$

$$Assuming\ B = B_0 Sin\ (\omega t)$$

$$E = -n * \pi r^2 \omega B_0 Cos(\omega t)$$

$$E_{max} = n\pi r^2 \omega\ B_{max}$$

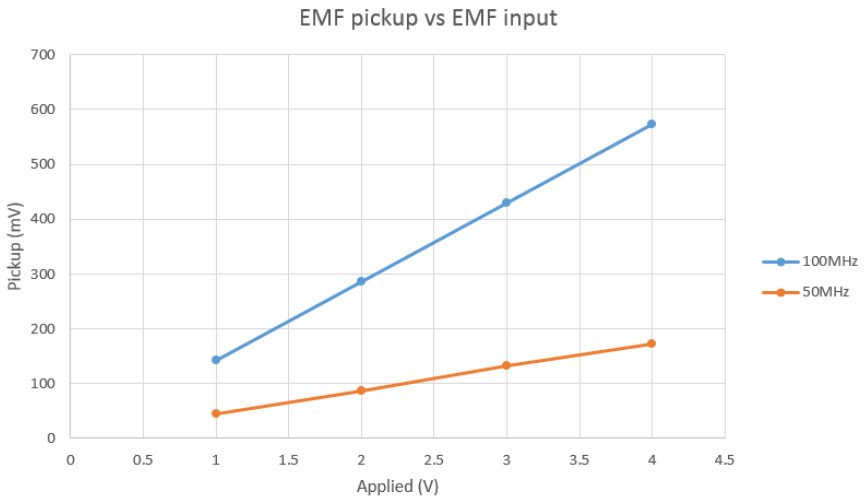

Figure 17 The field strength is indeed linear with input, and more power is reflected back to the source at 50MHz.

For 100 MHz, the EMF pickup along the z-direction was 575mV, while the pickup around the XY-plane was 150 to 250 mV. (as the coil normal was rotated along the XY-plane). The B-field was hence majorly found to lie along the z-direction.

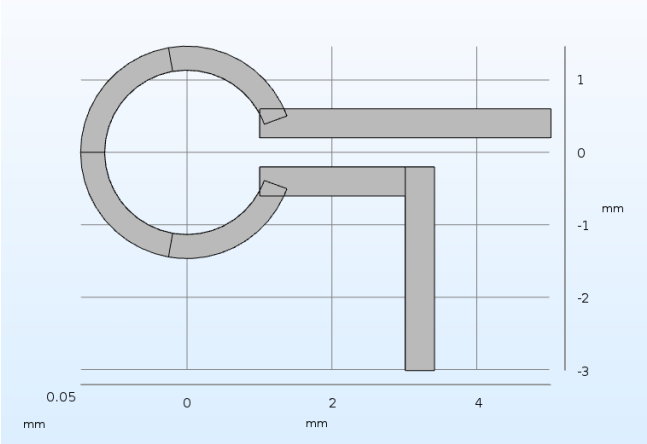

Figure 18 Earlier loop design

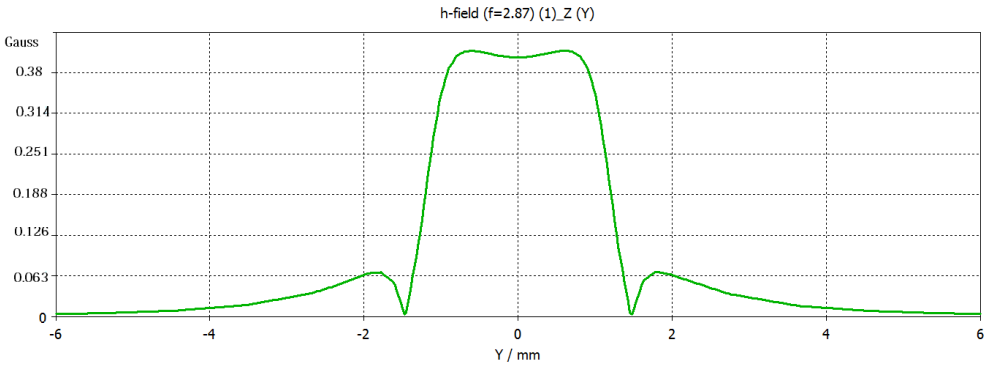

Figure 19 Bz along y for earlier design

Comparison

The results of the microstrip resonator were not found to be better than that from the earlier designs, which offered a ~1 mm radius circle region of uniformity.

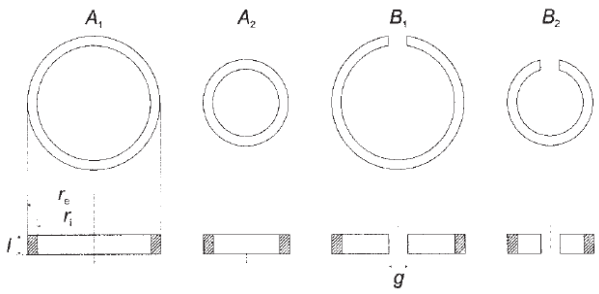

Figure 1 Schematic representation of the elements from which the resonators are constructed

Split Ring Resonator

The microstrip antenna discussed in the previous sections came with a severe drawback – the design had large amounts of copper, and copper scatters light at 637nm, and hence adds noise to the experiment. Hence, I repeated the experiments with a double split ring resonator[4].

Design method

The effectiveness of the Split Ring Resonator has been demonstrated in [3].

Bayat et al [3] reports measured values of Rabi nutation frequency to be fairly uniform over the entire measurement area (0.95 × 1.2 mm), in the range of 14.34–16.69 MHz as the objective is moved across the sample. Average magnetic field intensity was 5.59G at an input power of 0.5W

The feed line is capacitively coupled to the rings. The material used for the PCB is Rogers 6010.2L substrate.

Since the eventual goal is to design the antenna in ceramic PCB, the board has to be pretty much redesigned from scratch. (i.e. match the impedance. Since the electrical properties of ceramic are different from Rogers 6010.2L, simply copying the design dimensions is likely to lead to impedance mismatches)

Fortunately, there are analytical models for split ring resonators that date all the way back to 1981 through 1999. I used these expressions to estimate the split ring parameters, and fine-tuned them using CST Microwave studio.

[7] gives a neat synopsis of the analytical models for double split ring resonators. The outer and inner ring may be two among the following four prototypes-

ie. the design may have a closed outer ring and split inner ring (A1B2) or both rings split (B1B2). The analytical expressions for the two aforementioned cases are,

For A1B2

$$\omega_r = (c/r_{i2})(1 + r_{i2}^2/(r_{i1}^2 - r_{e2}^2))^{1/2}(g/\pi)^{1/2}(r_{e2} - r_{i2})^{-1/2}$$

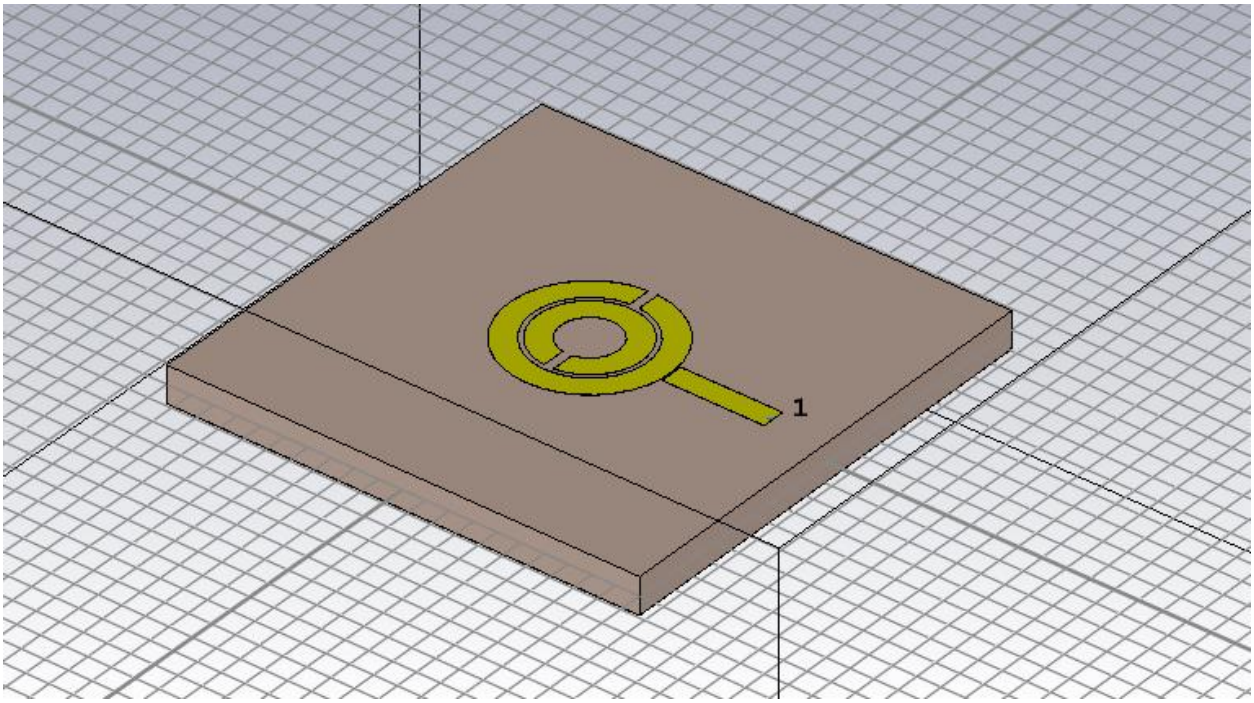

Figure 20 CST Microwave Studio model for split ring resonator

For B1B2

$$\omega_r = (3d/\pi^2 r)^{1/2}(c/r),$$

where

$$d = r_{i1} - r_{e2}, \quad r = (r_{i1} + r_{e2})/2.$$

Where r, c and g are the microstrip trace characteristics. This is explained in more detail in [7].

From theoretical considerations described in the linked papers, the field is expected to be uniform in the central circular region of the resonator.

Before printing the PCB on ceramic, it was prudent to verify the design flow by making an FR-4 prototype first. As per the availability of PCB material at the electronics lab in the Physics Department, the FR-4 thickness was modelled as 1.54mm. These were the parameter values tuned for good impedance matching at around 2.9GHz from the CAD tool. (all lengths are in mm)

Gs	0.4	Gap width at ring split
R1	2.2	Inner radius of smaller ring
R2	3.4	Inner radius of larger ring
Rt	1	Ring thickness
Gr	0.2	Gap between rings
w	1	Feed line width
Gc	0.05	Coupling gap to feed line
Fl	7	Feed line length

Notations as followed in [4]

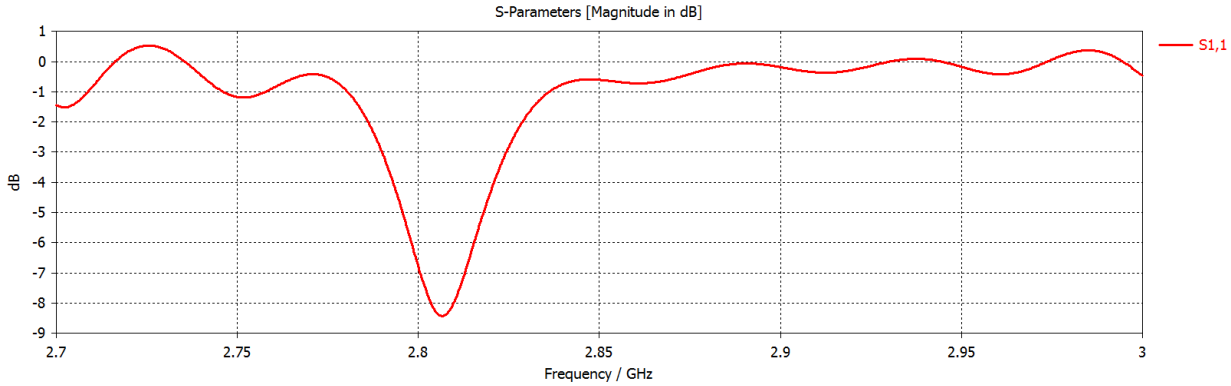

Figure 21 S11 parameter from the simulation

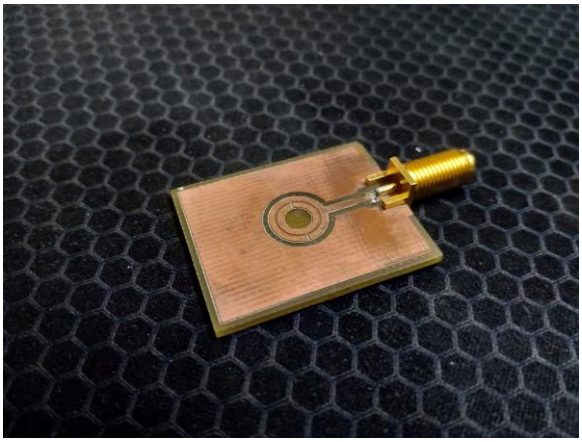

Figure 22 Fabricated PCB

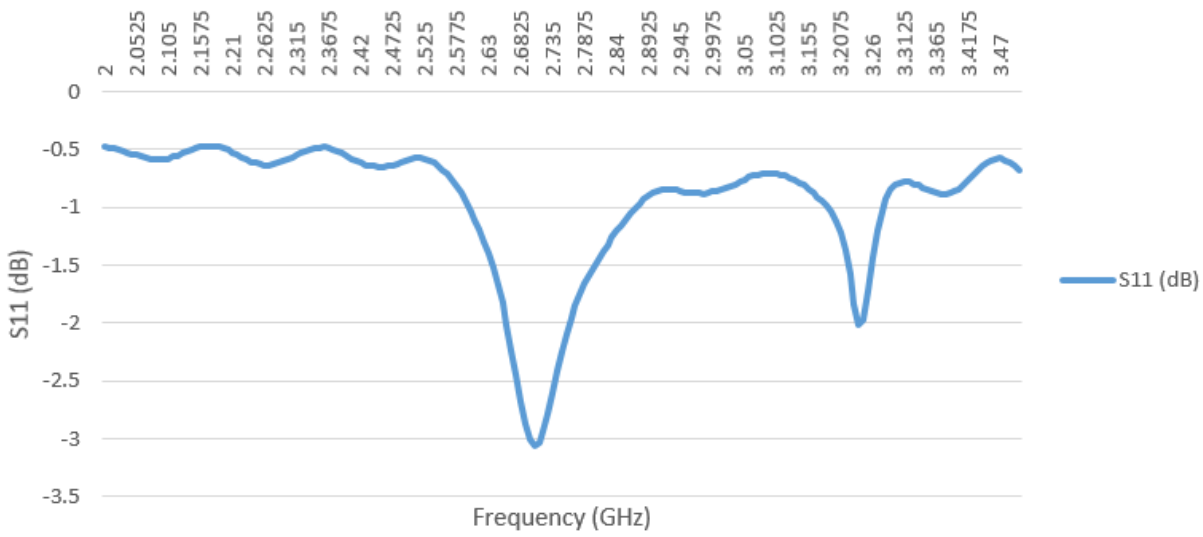

Figure 23 S11 parameter

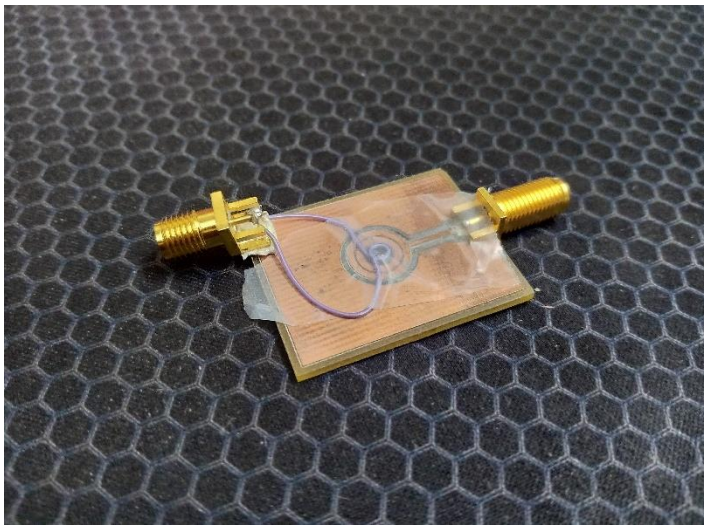

Figure 24 Measuring magnetic field

Fabrication and Testing

As before, to test the profile of magnetic field generated by the resonator, a small loop was used.

The measured field is found to be much lower than expected – Reasons could include high value of S11 or inductance of the coil used for measuring the field. (From the simulations, expected field strength was over 1 Gauss)

The reason for the enormous mismatch is strongly suspected to be the indeterminate impedance of the single loop coil used for measuring the field. It is not feasible to account for the impedance mismatch and factor it in by measuring the actual impedance of the loop because tiny errors in the impedance measurement leads to large differences in the correction factor.

However, assuming the simulations hold some merit, the correction factor can be estimated by comparing the measured field and the simulated field intensity. Once the correction factor is estimated, the entire field strength spectrum may be scaled up accordingly.

The field intensity for a 2.87 GHz signal of 1 V amplitude is simulated to be 0.63 Gauss.

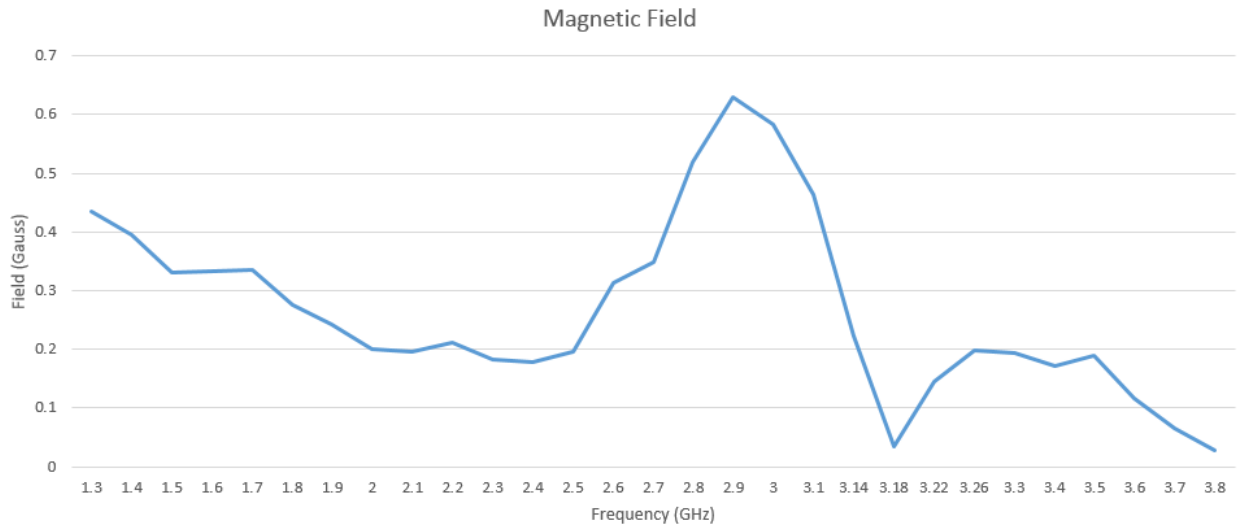

Figure 25 Measured Bz field, corrected for loop impedance mismatch

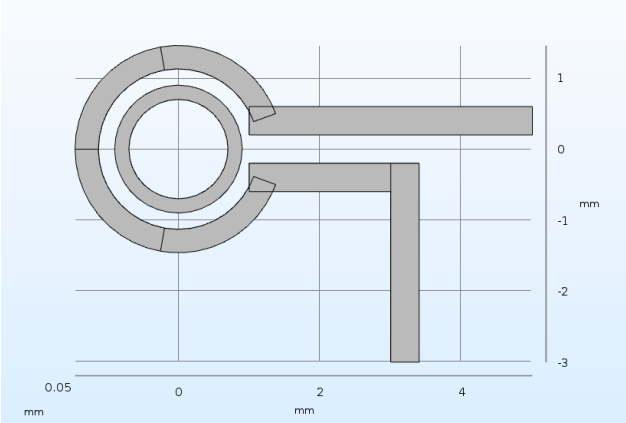

Figure 26 Previous design - with via

Comparison

In this section I have compared the performance of my split ring resonator design with the design that had been in use earlier within the group. I have compared the two most critical aspects of the design, in particular the field uniformity and the impedance matching.

Prof. Kasturi had simulated a couple of RF boards, notable among them the two designs below. These images below are from Prof. Kasturi's Comsol simulation files.

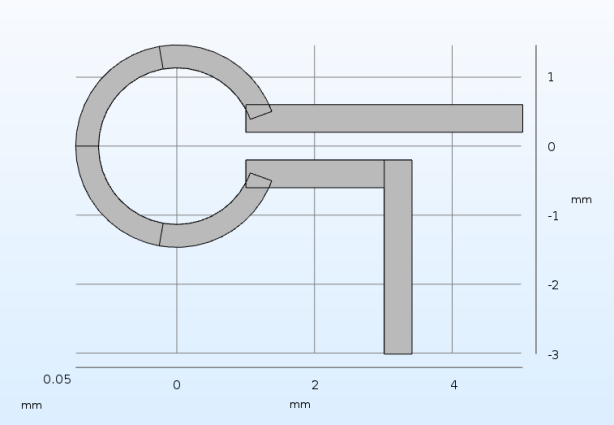

Figure 27 Previous design - without via

In the existing Comsol models for the older designs, the port type used is set to current port, with an amplitude of 0.5 A. This poses a severe problem in that if the design is poorly impedance matched, unfeasible levels of input voltages would be required to reach the target current.

I suspect that Comsol simply supplies whatever voltage amplitude is required to drive a 0.5 A current through the coil, and calculates the corresponding field strength. In practice, the power supply might be unable to provide the voltage levels required to drive 0.5 A through the coils.

To mitigate these issues, I exported these designs to CST Microwave studio, a specialized toolkit for RF design, with an arguably more efficient design flow and a relatively shallow learning curve. The S parameters and field strengths were monitored.

To properly account for any nonlinear effects, I have used a time domain simulation instead of the frequency domain computations employed in Comsol. At the cost of slightly higher computational complexity, the nonlinear effects, if any are very well accounted for in time domain studies.

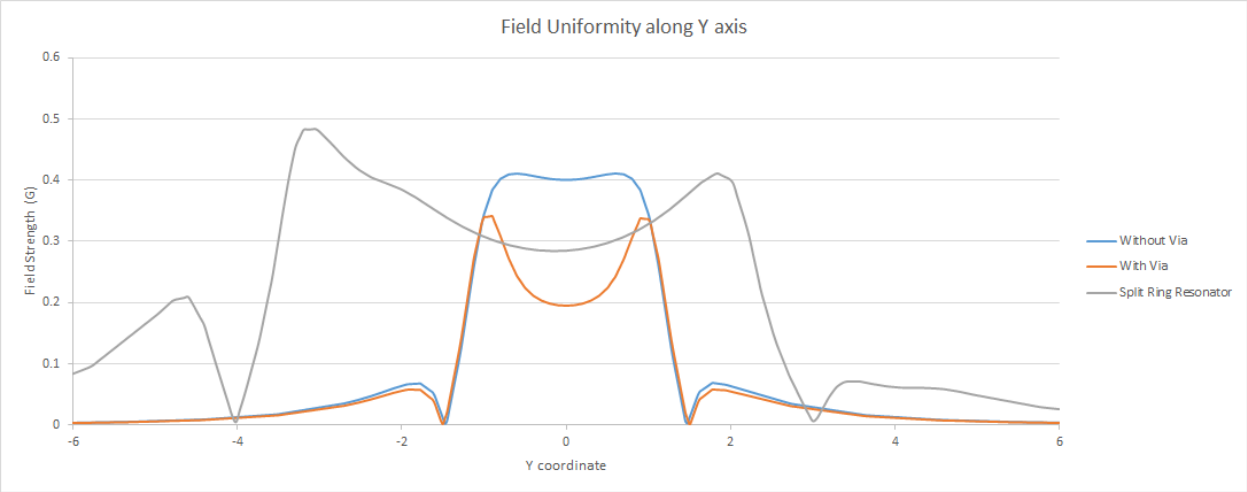

Figure 28 Field along y axis, 0.5 mm above the PCB

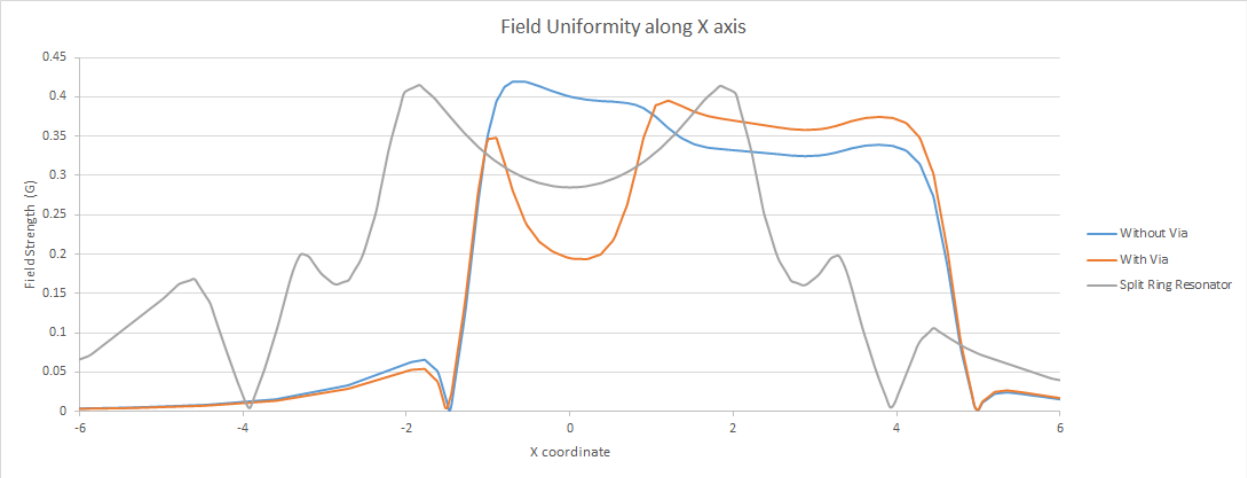

Figure 29 Field along x axis, 0.5 mm above the PCB

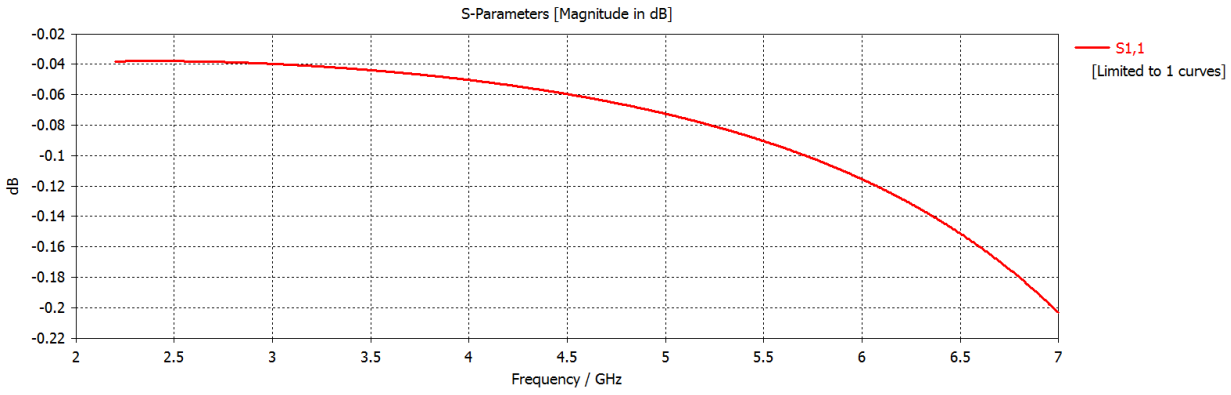

Figure 30 S11 for loop with via

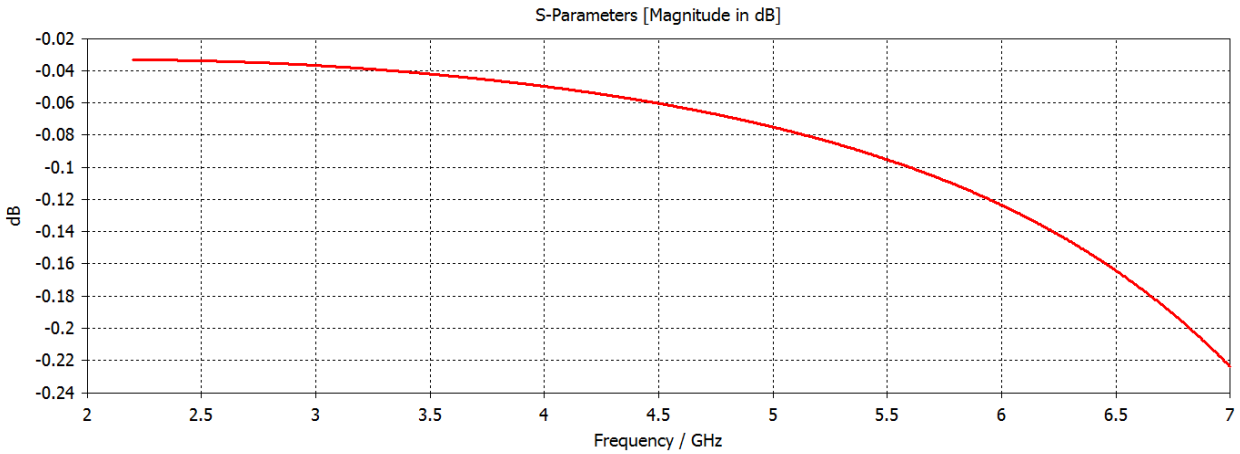

Figure 31 S11 for loop without via

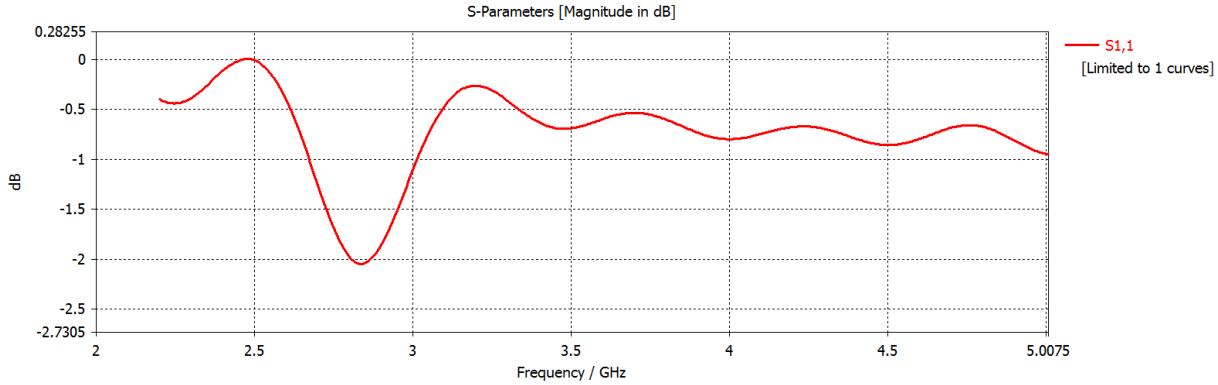

Figure 32 S11 for Split Ring Resonator

In [4], the variation of Hz along x, y, and z directions over 1.5 × 1.5 mm area and thickness of 0.5 mm is less than 6.5%, 10%, and 1%, respectively. Taking similar tolerance limits, the available area for the diamond sample is a circle with a radius 1.13mm, nearly 4 sq. mm. This is a 57% increase in area from the previous design, corresponding to a shot noise limited sensitivity of 21%.

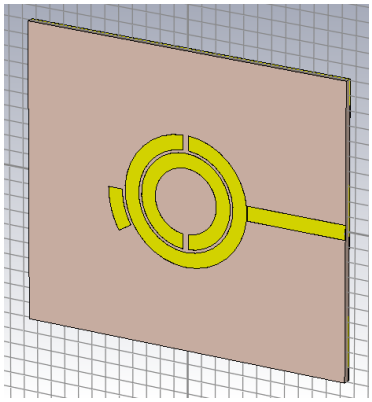

Figure 33 One possible way to add capacitance

Ceramic Substrate

Due to the attractive thermal and optical properties of Alumina, we initially planned to prototype the boards in Ceramic substrate. However, for similar values of split ring radii, the resonator is tuned to nearly 7 GHz (due to the higher permittivity). Playing around with the analytical and CST models, the resonant frequency can be lowered by increasing the loop radii.

Unfortunately, when the loop radius is increased beyond 2mm, the field uniformity in the center essentially vanishes, rendering the entire design useless. To overcome this difficulty, I have tried various ways of adding/removing capacitance/inductance – for instance adding or removing one split ring, coupled stub capacitance, etc. Some of these techniques were indeed effective at bringing down the resonance frequency, but also led to severe deterioration of the quality of resonance.

References

[1] M. Hirose, “Quantum Control of Spin Systems in Diamond,” *Thesis*, no. 2009, 2015.

[2] L. Robledo, H. Bernien, T. Van Der Sar, and R. Hanson, “Spin dynamics in the optical cycle of single nitrogen-vacancy centres in diamond,” *New J. Phys.*, vol. 13, 2011.

[3] L. M. Pham, “Magnetic Field Sensing with Nitrogen-Vacancy Color Centers in Diamond,” *PhD thesis*, vol. PhD thesis, no. May, 2013.

[4] K. Bayat, J. Choy, M. Farrokh Baroughi, S. Meesala, and M. Loncar, “Efficient, uniform, and large area microwave magnetic coupling to NV centers in diamond using double split-ring resonators,” *Nano Lett.*, vol. 14, no. 3, pp. 1208–1213, 2014.

[5] K. Sasaki *et al.*, “Broadband, large-area microwave antenna for optically-detected magnetic resonance of nitrogen-vacancy centers in diamond,” no. iii, pp. 1–6, 2016.

[6] L. Qin *et al.*, “Near-field microwave radiation function on spin assembly of nitrogen vacancy centers in diamond with copper wire and ring microstrip antennas,” *Jpn. J. Appl. Phys.*, vol. 57, no. 7, pp. 1–7, 2018.

[7] A. Radkovskaya *et al.*, “Resonant frequencies of a combination of split rings: Experimental, analytical and numerical study,” *Microw. Opt. Technol. Lett.*, vol. 46, no. 5, pp. 473–476, 2005.